THE ASTROPHYSICAL JOURNAL, 312:344–350, 1987 January 1

SUBMILLIMETER SPECTRAL LINE OBSERVATIONS IN VERY DENSE REGIONS

NEAL J. EVANS II
Department of Astronomy, and Electrical Engineering Research Laboratory, The University of Texas at Austin
LEE G. MUNDY
Department of Astronomy and Electrical Engineering Research Laboratory, The University of Texas at Austin, and Owens Valley Radio Observatory, California Institute of Technology
JOHN H. DAVIS
Electrical Engineering Research Laboratory, and Department of Electrical and Computer Engineering, The University of Texas at Austin
AND
PAUL VANDEN BOUT
Department of Astronomy, and Electrical Engineering Research Laboratory, The University of Texas at Austin, and National Radio Astronomy Observatory[1]
Received 1986 March 24; accepted 1986 June 10

ABSTRACT

In a search for very high density ($n \gg 10^6$ cm^{-3}) regions, the Millimeter Wave Observatory 5 m telescope was used to observe several submillimeter lines. The cores of M17, S140, and NGC 2024 were observed in the CS($J = 7 \rightarrow 6$), $H_2CO(J_{K-1K1} = 5_{15} \rightarrow 4_{14})$, and HCN($J = 4 \rightarrow 3$) lines. These data are combined with data at millimeter wavelengths to derive the volume density, and the results are compared to those deduced from millimeter lines alone (Snell *et al.* 1984; Mundy *et al.* 1986*a*, *b*). If only the highest excitation CS and H_2CO lines are compared, there is evidence for some densities up to about 10^7 cm^{-3}, but the uncertainties are large. When combined with the entire data set of lower J transitions, the submillimeter lines are generally consistent with the results of Snell *et al.* (1984) and Mundy *et al.*, indicating densities of $\sim 10^6$ cm^{-3}.

Subject heading: interstellar: molecules

I. INTRODUCTION

Current observations of molecular clouds and star formation are intriguingly incomplete in tracing the evolutionary sequence from low-density molecular cloud to pre–main-sequence star. The progression from molecular gas to stars is fundamentally a progression to smaller size scales and higher densities. In molecular clouds, we can easily observe the first steps of this progression. Molecular gas in the extended envelopes of clouds has density $\sim$100–1000 cm^{-3}; gas in parsec-scale condensations can be found with $n \sim 10^4$–10^5 cm^{-3}; and gas in the dense cores of clouds with OB star formation has $n \sim 10^6$ cm^{-3}. It is also easy to observe the end products of the process, pre–main-sequence stars. What is missing from the observational ledgers is the intermediate state, very high density ($n \gg 10^6$ cm^{-3}) condensations. It can be argued that the lifetime against gravitational collapse of such objects is very short, making them extremely rare. On the other hand, we see on all larger scales more gas than expected from this time scale argument; thus the crucial question becomes the following. At what density do gas condensations begin to collapse on a free-fall time scale? To answer this question, we must develop ways to search for condensations with $n > 10^6$ cm^{-3}.

The utility of multitransitional studies of CS in determining the conditions in molecular clouds has been demonstrated by Snell *et al.* (1984) and Mundy *et al.* (1986*a*). A similar analysis has been applied to H_2CO (Mundy *et al.* 1986*b*). These studies have revealed the presence of dense gas ($n \sim 10^6$ cm^{-3}) in the cores of molecular clouds with are forming stars. While the emission is extended over several beam diameters, many aspects of the data are best explained in a model with many small, dense clumps. These may be protostellar condensations, and their high density suggests that the evolutionary time scales may be short.

The studies referenced above do not strongly constrain the existence of still higher density gas. They are based on transitions ranging in wavelength from 1 to 3 mm, with the shortest wavelength corresponding to the $J = 6 \rightarrow 5$ transitions of CS. To test for still higher densities, we have observed these regions at submillimeter wavelengths. By going to shorter wavelengths we are able to study higher rotational transitions which in turn are excited only in extremely dense regions. In addition to observing the $J = 7 \rightarrow 6$ transition of CS and the $J_{K-1K1} = 5_{15} \rightarrow 4_{14}$ transition of H_2CO, we have observed the $J = 3 \rightarrow 2$ and $4 \rightarrow 3$ transitions of HCN. The characteristic density of the observed transitions is given in Table 1, along with the frequency and energy above the ground state.

II. OBSERVATIONS

Observations were obtained with the 5 m antenna of the Millimeter Wave Observatory[2] (MWO) of the University of Texas at Austin. The observations were obtained before the installation of error-correcting optics which have substantially reduced the beam sizes and increased the efficiencies compared to the values given in the table. The efficiencies are given for uniform sources of both 2′ and 3′ extent. The sub-mm receiver was a cooled Schottky diode mixer similar to that described by Erickson (1981). The SSB receiver temperature was $\sim$3000 K; the system temperature was dominated by atmospheric opacity and varied from 5000 K to >10,000 K at $\sim$350 GHz.

[1] National Radio Astronomy Observatory, operated by Associated Universities, Inc., under contract with the National Science Foundation.

[2] The Millimeter Wave Observatory is operated by the Electrical Engineering Research Laboratory of The University of Texas at Austin with support from the National Science Foundation and McDonald Observatory.

TABLE 1

OBSERVED LINES

Species	Transition	Frequency (GHz)	n^* (cm^{-3})	E_u (K)	Beam Size (arcsec)	$\eta(2')$	$\eta(3')$
HCN	$3 \rightarrow 2$	265.886	7.2×10^7	26	75	0.40	0.53
H_2CO	$4_{14} \rightarrow 3_{13}$	281.527	1.2×10^7	31	73	0.38	0.51
CS	$6 \rightarrow 5$	293.912	1.2×10^7	49	72	0.36	0.49
CS	$7 \rightarrow 6$	342.883	2.2×10^7	66	73	0.33	0.47
H_2CO	$5_{15} \rightarrow 4_{14}$	351.769	2.6×10^7	47	73	0.32	0.46
HCN	$4 \rightarrow 3$	354.505	1.6×10^8	43	73	0.32	0.46

The data were calibrated by the usual chopper wheel technique and the two-layer atmospheric model of Kutner (1978).

The data were corrected for telescope efficiency using a Ruze model (Ruze 1966) to describe the error pattern. The parameters of the model were fitted to measurements of Venus and the Moon acquired during the observing period. Previous information about the telescope error pattern at 210–280 GHz was also used. The fraction of the forward power contained in the main beam (η_B/η_l) was measured to be 0.27 ± 0.03 [assuming T_b (Venus) = 300 K] and the fractional power coupling to the Moon (η_{FSS}) was 0.83 ± 0.04. The data in Tables 2 and 3 are corrected using η_{FSS}. The cloud modeling in subsequent sections requires the data to be further corrected for antenna coupling to the source. The antenna efficiencies for uniform 2′ and 3′ diameter sources were calculated using the Ruze model. Since the densities derived by applying the alternative efficiences were within the measurement errors, we have chosen to present the results for only the 3′ efficiencies. This choice of source diameter gives consistency with previous multitransition studies of the observed sources (Snell *et al.* 1984; Mundy *et al.* 1986*a*, *b*).

III. RESULTS

Examples of the spectra are shown in Figure 1. The line parameters for all observed positions are given in Tables 2 and 3. Typical line temperatures are $T_R^* = 1$–3 K; central velocities and line widths of CS lines are in general agreement with those found by Snell *et al.* (1984). The limited maps in the CS $J = 7 \rightarrow 6$ transitions are consistent with the more detailed maps obtained in the lower CS transitions by Snell *et al.* (1984).

TABLE 2

HCN OBSERVATIONS

Position (E, N) (arcmin)	$J = 3 \rightarrow 2$				$J = 4 \rightarrow 3$			
	T^*_R (K)	V_{LSR} (km s^{-1})	ΔV (km s^{-1})	RMS (K)	T^*_R (K)	V_{LSR} (km s^{-1})	ΔV (km s^{-1})	RMS (K)
M17 (1, 2)	3.9	20.2	8.4	0.17	2.3	20.7	6.6	0.25
(1, 1)	3.3	19.8	8.4	0.17	1.9	19.9	8.2	0.29
(1, 0)	2.3	19.5	7.8	0.18	1.4	17.8	6.7	0.25
(0, 2)	2.5	20.8	8.8	0.18	1.2	21.1	6.8	0.45
(0, 1)	2.7	20.8	8.2	0.13	1.7	20.6	6.2	0.31
(0, 0)	1.6	20.1	8.2	0.17	1.4	18.4	5.6	0.41
S140 (0, 0)	2.5	−6.7	4.9	0.13	0.8	−6.9	2.2	0.42
NGC 2024 (0, 1)	3.6	11.3	2.7	0.24	1.4	10.8	2.6	0.40
(0, 0)	2.6	11.6	3.4	0.24	2.0	11.4	2.5	0.41
(0, −1)	1.7	11.5	3.6	0.20	1.2	11.1	2.8	0.40

TABLE 3

CS AND H_2CO OBSERVATIONS

Position (E, N) (arcmin)	CS $J = 7 \rightarrow 6$				H_2CO $5_{15} \rightarrow 4_{14}$			
	T^*_R (K)	V_{LSR} (km s^{-1})	ΔV (km s^{-1})	RMS (K)	T^*_R (K)	V_{LSR} (km s^{-1})	ΔV (km s^{-1})	RMS (K)
M17 (1, 2)	2.8	20.3	4.6	0.66	1.0	18.8	5.4	0.25
(1, 1)	2.9	19.8	5.6	0.46	1.2	19.2	5.0	0.29
(1, 0)	2.8	19.1	5.3	0.36	<0.5	...	...	0.25
(0, 2)	...	...	...	...	<0.6	...	...	0.45
(0, 1)	1.6	20.5	5.0	0.34	<0.5	...	...	0.33
(0, 0)	1.3	20.5	6.3	0.36	<0.7	...	...	0.42
S140 (0, 0)	0.4	−7.4	2.3	0.30	<0.3	...	...	0.20
NGC 2024 (0.7, 0)	1.9	11.2	0.8	0.70	<0.5	...	...	...
(0, 2)	1.4	10.5	1.9	0.53	<0.5	...	...	...
(0, 1)	2.0	10.7	1.8	0.42	<0.5	...	...	...
(0, 0)	2.2	10.9	2.1	0.40	<0.5	...	...	...
(0, −1)	2.0	11.0	2.3	0.39	>0.5	...	...	...
(0, −2)	0.8	11.1	1.9	0.45	<0.5	...	...	...
(−0.7, 0)	1.6	11.0	2.0	0.59	<0.5	...	...	...

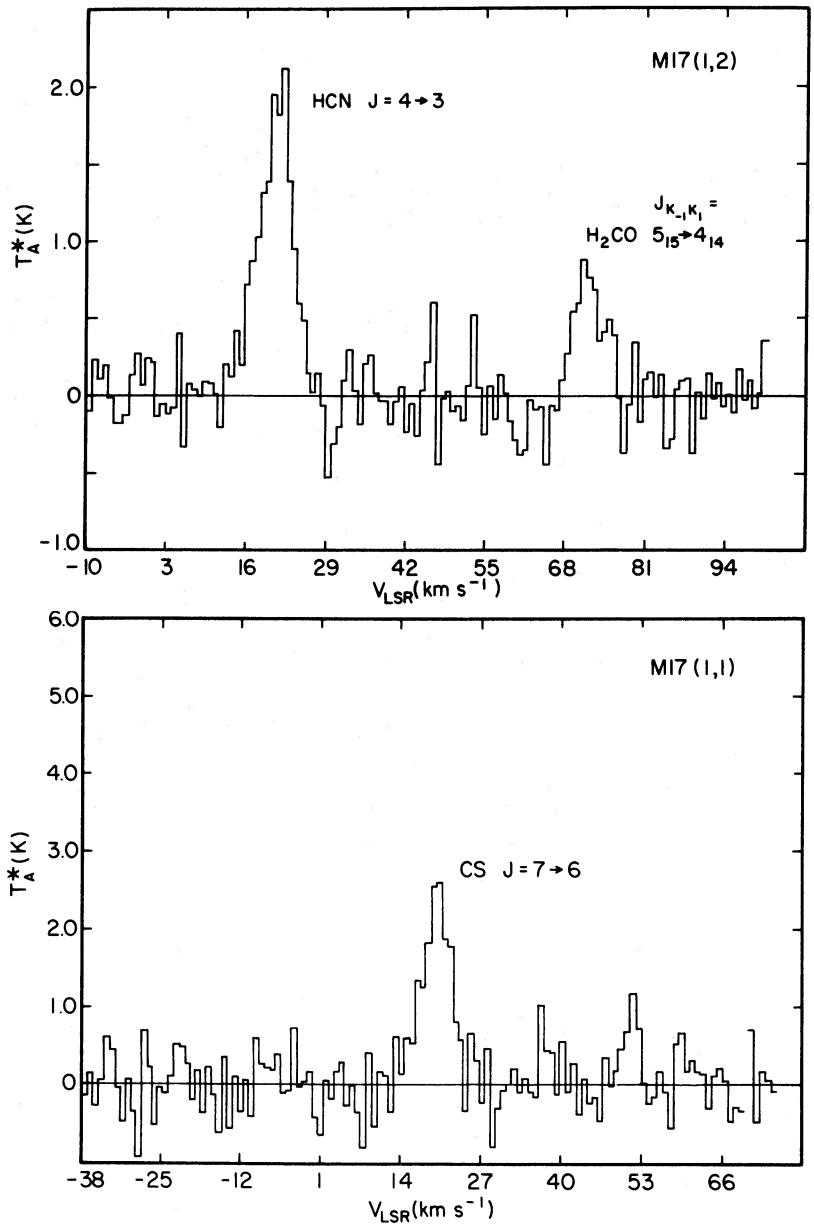

FIG. 1.—Spectra of M17 are presented. The upper spectrum shows the HCN $J = 4 \rightarrow 3$ and H_2CO $J_{K-1K1} = 5_{15} \rightarrow 4_{14}$ transitions at position (1, 2). The velocity scale is correct only for the HCN line. The bottom figure is the CS $J = 7 \rightarrow 6$ line at position (1, 1). The vertical axis is T^*_A (i.e., not corrected for η_{FSS}).

Furthermore, the line temperatures of the CS $J = 7 \rightarrow 6$ line in M17 are in excellent agreement with those seen by Snell *et al.* (1986) using the MMT.

A fortunate frequency coincidence allows us to observe HCN $J = 4 \rightarrow 3$ and H_2CO $J_{K-1K1} = 5_{15}$–4_{14} simultaneously in opposite sidebands (see Fig. 1). Contour maps of the $J = 3 \rightarrow 2$ HCN emission are shown for the three sources in Figure 2. The source sizes and morphologies are similar to those seen in the high excitation lines of CS (Snell *et al.* 1984) and H_2CO (Mundy *et al.* 1986*b*).

IV. DISCUSSION

To analyze the data, we have produced grids of large velocity gradient (LVG) models as described in Snell *et al.* (1984). Analysis of other radiative transport models indicates that our choice of the LVG model has little effect on the derived densities (Snell *et al.* 1984; Mundy 1984). From the grids of models we can produce plots which show line ratios and line temperatures which can be used to derive densities (n) and molecular column densities (N). In Figure 3, we present four of these plots in which the dashed lines indicated the ratios of two lines and solid lines indicate the temperature of one of the lines. Since the relevant quantity for determining the importance of trapping is the column density per unit velocity interval, the horizontal axis is log ($N/\Delta v$), where Δv is the line width. The vertical axis is the log of the density. The virtues and limitations of using various pairs of lines are illustrated in Figure 3. Where the dashed lines are mostly perpendicular to the solid lines, the two transitions provide a good density probe; where the lines are relatively parallel, the density will not be well defined. Another aspect to consider is the spacing of the contour levels, since these also control how a given observa-

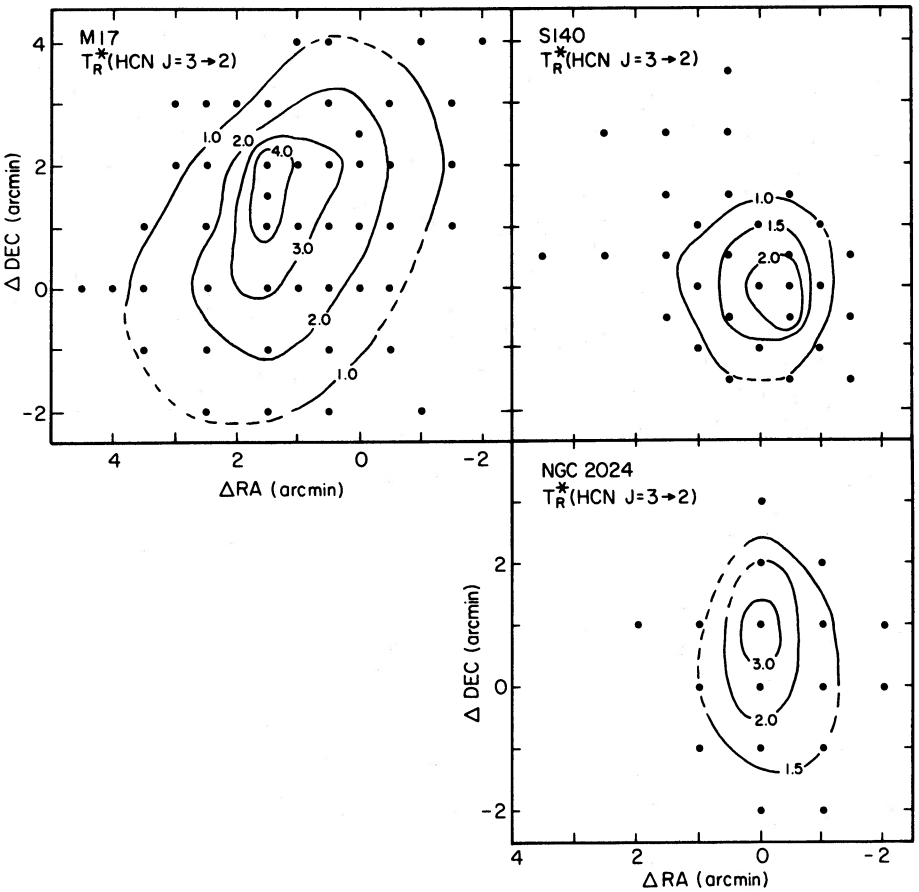

FIG. 2.—Maps of M17, S140, and NGC 2024 in the HCN $J = 3 \rightarrow 2$ line are shown. The contours are lines of equal T^*_R (corrected for η_{FSS}), and the dots show where data were taken. Offsets are relative to these 1950 coordinates: $\alpha = 18^h17^m27^s$, $\delta = -16°14'55''$ (M17); $\alpha = 22^h17^m42^s$, $\delta = 63°03'45''$(S140); $\alpha = 05^h39^m13^s$, $\delta = -01°56'58''$ (NGC 2024).

tional uncertainty will translate into uncertainties in density and column density. Comparing the two left-hand panels, we find the the CS $J = 2 \rightarrow 1$ and $7 \rightarrow 6$ transitions will produce densities with small uncertainties because the ratio of line temperatures varies rapidly with density. This rapid variation is caused by the large difference in characteristic densities ($n^* = 5.7 \times 10^5$ cm^{-3} for $J = 2 \rightarrow 1$ and $n^* = 2.2 \times 10^7$ cm^{-3} for $J = 7 \rightarrow 6$), a feature we will describe as a "long lever arm." Conversely, the $J = 7 \rightarrow 6$ and $J = 6 \rightarrow 5$ lines have more similar n^*, a "short lever arm"; thus a small observational error translates into a large uncertainty in density. As compensation, the lines remain perpendicular in the $J = 7 \rightarrow 6$ and $6 \rightarrow 5$ diagram in some regions where they become nearly parallel in the $J = 7 \rightarrow 6$ and $2 \rightarrow 1$ diagram. Similar remarks apply to the corresponding diagrams for H_2CO shown in the two panels on the right.

The solutions for several positions in M17 are plotted in Figure 3 and serve to illustrate the points made above. The error ellipses for the transitions with short lever arms are very elongated. In particular, the lower bounds to the density are indeterminate. This indeterminancy arises because the excitation caused by photon trapping is difficult to distinguish from that caused by collisions in these high J lines. The main virtue of these pairs of transitions is to provide an upper limit to the densities. In contrast, the transitions with long lever arms produce small error ellipses in Figure 3. It is in this context that we must regard the density estimates presented in Table 4. These densities are all quite high but they are also quite uncertain especially with regard to the lower limit.

Densities derived from the HCN $J = 4 \rightarrow 3$ and $3 \rightarrow 2$ lines are also presented in Table 4. The uncertainties are considerably less for these density determinations and, most importantly, all but two positions have both upper and lower bounds. The reason that HCN yields better results is not that its

TABLE 4

LOG OF DENSITIES DERIVED FROM SUBMILLIMETER LINES

Position	CS $7 \rightarrow 6$ & $6 \rightarrow 5$	H_2CO 280 & 350	HCN $4 \rightarrow 3$ & $3 \rightarrow 2$
M17 (1, 2)	$6.8^a - 0.8$	$6.2 + 0.4$	6.7 ± 0.3
(1, 1)	$6.2 + 0.6$	$6.1 + 0.5$	6.7 ± 0.3
(1, 0)	$7.1^a + 0.8$	...[b]	6.8 ± 0.3
(0, 2)	...[b]	...[b]	$6.5^a + 0.5$
(0, 1)	< 5.9	...[b]	6.9 ± 0.3
(0, 0)	$6.2^a + 0.5$	...[b]	$7.3^a - 0.5$
S140 (0, 0)	...[c]	...[b]	$6.4^a + 0.5$
NGC 2024 (0, 2)	> 7.0	...[b]	...[b]
(0, 1)	> 6.6	...[b]	$6.2^a + 0.6$
(0, 0)	$6.7^a - 0.4$	...[b]	7.3 ± 0.6
(0, −1)	$7.4^a - 0.6$	...[b]	7.2 ± 0.7
(0, −2)	...[b]	...[b]	...[b]

[a] Where one-sided uncertainties are given, there is essentially no constraint in the other direction.

[b] No data at this position for at least one of the lines.

[c] No solution.

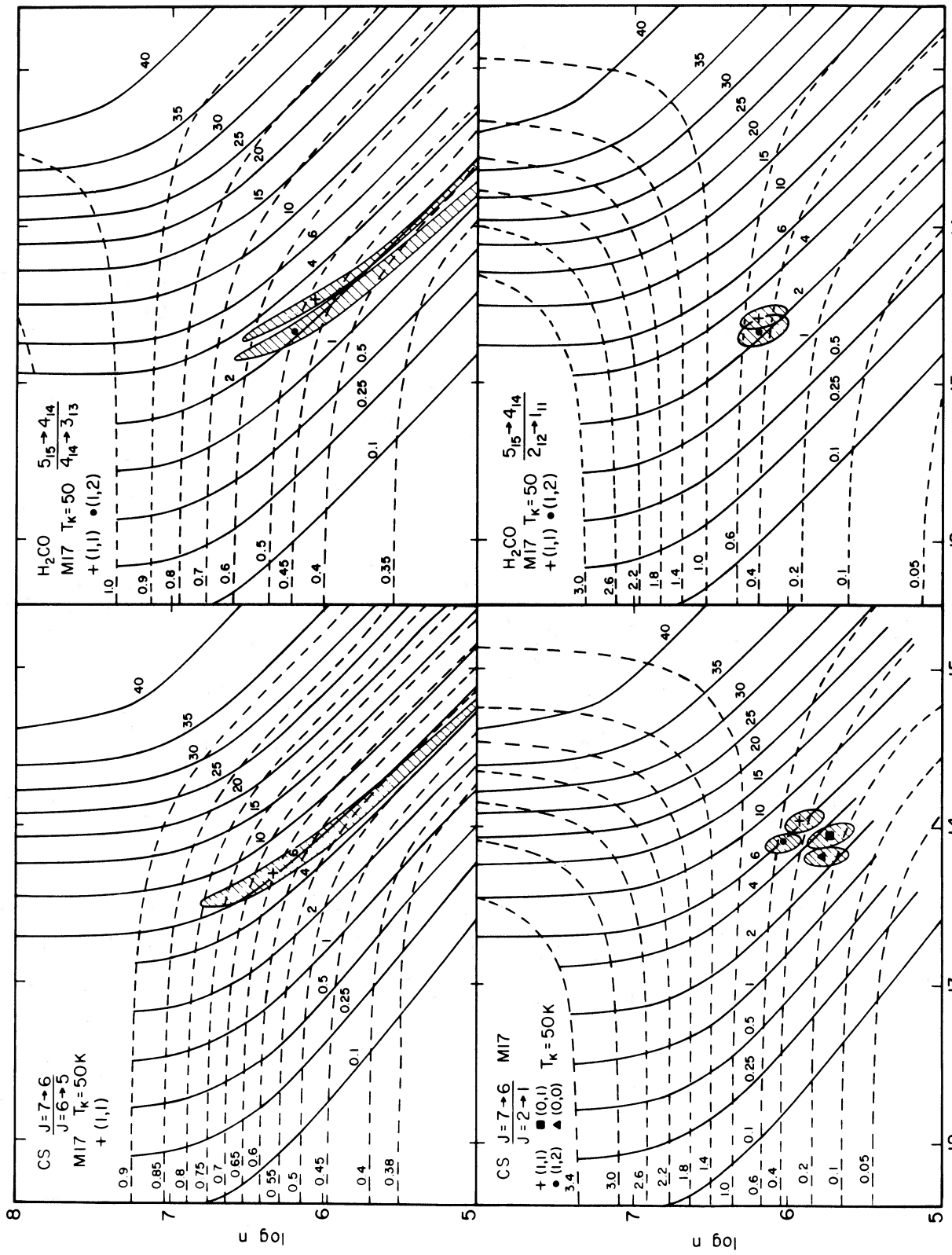

FIG. 3.—The four panels show grids from the LVG models. All models shown were run at $T_k = 50$ K, appropriate for M17. The vertical axes are log of the density and the horizontal axes are log of the molecular column density divided by the linewidth. The solid lines are contours of constant radiation temperature (T_R) for the $J = 7 \rightarrow 6$ line (CS) or the $J_{K-1K1} = 5_{15} \rightarrow 4_{14}$ line (H_2CO). The dashed contours are lines of constant ratio of two lines as indicated in each figure. Exemplary solutions for the several points in M17 are shown by the symbols and error ellipses. The symbols' correspondence to positions is shown in the figure.

diagram is much different from those of CS or H_2CO, but that the uncertainties on the line strengths are less. Consequently, there is some hope of improving the n determinations from CS and H_2CO if spectra are obtained with better signal-to-noise ratio. The densities derived from HCN are large, generally $>10^6$ cm^{-3} and sometimes greater than 10^7, although the latter tend to have larger uncertainties.

On the source-by-source basis, we find that S140 shows no clear evidence for densities greater than 10^6 cm^{-3}. In M17, $n > 10^6$ cm^{-3} are indicated at all positions, but except for the HCN, the uncertainties overlap the solutions of Snell *et al.* (1984). In NGC 2024, the evidence for higher densities is somewhat more convincing at four positions; the lower limit to n derived from CS is clearly larger than that found by Snell *et al.*

We have also derived densities based on the long-lever arm pairs of transitions shown in Figure 3. The results are shown in Table 5. As shown by the small error ellipses in Figure 3, the uncertainties on these densities are much less. The derived densities are also lower than those in Table 4, which were based on the short lever arm pairs of transitions. Also presented in Table 5 are the densities derived from previous fits to multiple transitions of CS (Snell *et al.* 1984) and H_2CO (Mundy *et al.* 1986*b*). The current results are somewhat higher than those from multitransition fits, but the error bars usually overlap.

Finally, we have included the sub-mm transitions with the previous multitransition data to produce a fit to the full data set. The densities derived in this way are also presented in Table 5. As one might expect, they tend to lie between the densities derived by Snell *et al.* (1984) or Mundy *et al.* (1986*b*)

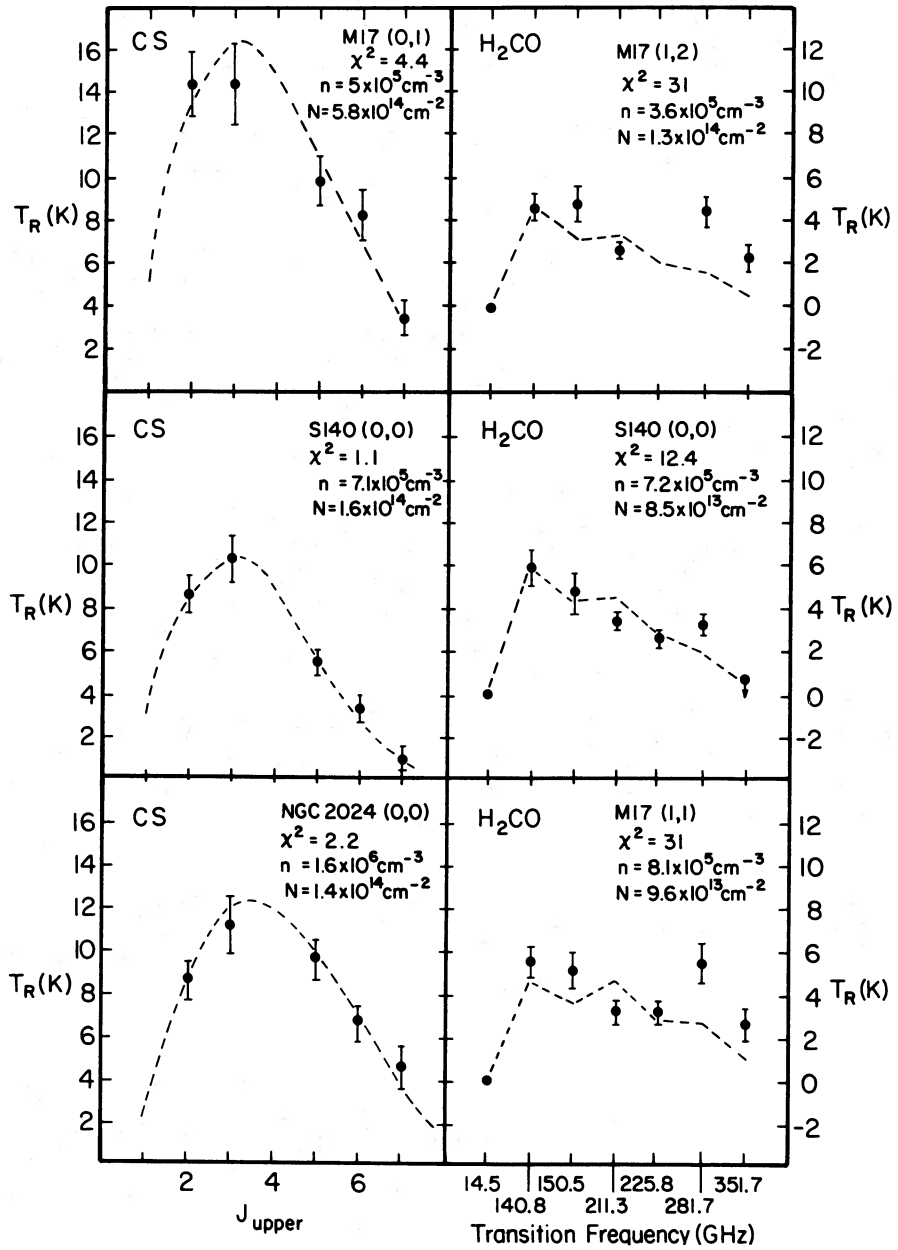

FIG. 4.—The CS (*left side*) or H_2CO (*right side*) radiation temperatures (T_R) are shown for several positions along with the predictions from the best-fitting model (*dashed lines*). One position from each source is shown for CS, but two positions from M17 are shown for H_2CO. In S140 the H_2CO model fit is from Mundy *et al.* (1986) and the upper limit to the 351.7 GHz line is shown to test compatibility with this model.

TABLE 5

LOG OF DERIVED DENSITIES

Position	CS $7 \rightarrow 6$ & $2 \rightarrow 1$	CS full fit	CS Snell *et al.* (1984)	H_2CO 350 & 140	H_2CO full fit	H_2CO Mundy *et al.* (1986)
			M17			
(1, 2)	6.0 ± 0.1	6.0[a]	5.9[a]	6.2 ± 0.2	5.6[a]	5.5 ± 0.2
(1, 1)	5.9 ± 0.1	5.8[a]	5.7[a]	6.2 ± 0.1	5.9[a]	5.8 ± 0.2
(1, 0)	5.9 ± 0.2	5.8 ± 0.1	5.5 ± 0.1	...[b]	...[b]	5.7 ± 0.1
(0, 1)	5.7 ± 0.2	5.7 ± 0.1	5.7 ± 0.1	...[b]	...[b]	5.6 ± 0.2
(0, 0)	5.8 ± 0.2	5.7 ± 0.1	5.6 ± 0.1	...[b]	...[b]	5.6 ± 0.2
			S140			
(0, 0)	5.7 ± 0.2	5.9 ± 0.1	5.9 ± 0.1	...[b]	...[b]	5.9 ± 0.1
			NGC 2024			
(0, 2)	6.4 ± 0.2	6.2 ± 0.1	6.2 ± 0.1	...[b]	...[b]	6.3 ± 0.2
(0, 1)	6.2 ± 0.2	6.2[a]	6.2[a]	...[b]	...[b]	5.9 ± 0.2
(0, 0)	6.2 ± 0.1	6.2 ± 0.1	6.2 ± 0.1	...[b]	...[b]	6.0 ± 0.1
(0, −1)	6.2 ± 0.2	6.1 ± 0.1	6.0 ± 0.1	...[b]	...[b]	5.9 ± 0.1
(0, −2)	6.0 ± 0.2	5.7 ± 0.1[c]	5.7 ± 0.1	...[b]	...[b]	5.4 ± 0.5

[a] χ^2 indicates that the model does not adequately fit the data; in this case no error bars are assigned.
[b] 351.8 GHz line not detected at this position.
[c] No $J = 6 \rightarrow 5$ data exist at this point.

and those derived using one sub-mm and one millimeter wavelength line. The densities derived by Snell *et al.* (1986) from the CS $J = 7 \rightarrow 6$ and $J = 4 \rightarrow 3$ lines tend to lie between those in Table 4 and those in Table 5. Comparisons of the data to the best fitting models are shown in Figure 4 for a selection of positions. In general, the sub-mm transitions are consistent with the best fitting model; there is little evidence in these plots for a separate component of much higher density. S140 maintains its record as the best-behaved of the sources.

The H_2CO fits in Figure 4 are in general less satisfactory than the CS fits. As discussed by Mundy *et al.* (1986*b*), this can be explained by attenuation of the intermediate frequency transitions (especially the 211.3 GHz line) by lower density foreground gas. The $5_{15} \rightarrow 4_{14}$ (351.7 GHz) transition supports this interpretation since it continues the tendency for the higher and lower frequency transitions to lie above the model fit. The inclusion of the intermediate frequency lines in the fit usually causes an underestimate of the density. This effect would explain the fact that the n from the H_2CO fits in Table 5 are often the lowest estimates.

In this section, we have discussed density determinations in the context of our simple source model, a uniform density region filling the beam which can be modeled adequately by the large-velocity-gradient approximation. The reader should bear in mind that deviations of the actual source from this simple model are an additional source of uncertainties (see, e.g., Mundy 1984).

V. CONCLUSIONS

The sub-mm transitions, analyzed by themselves, indicate that densities $\sim 10^7$ cm^{-3} may exist in the cores of the three molecular clouds studied here. At present, the uncertainties in this analysis are large. Comparisons of the sub-mm data with millimeter transitions or inclusion of the sub-mm data into full, multitransition data sets result in derived densities that are lower ($n \sim 10^6$ cm^{-3}) than those derived solely using sub-mm transitions. These lower densities are in agreement with previous results for CS and H_2CO (Snell *et al.* 1984; Mundy *et al.* 1986*b*). For this reason, we are inclined to prefer the densities given in Table 5, expecially those for CS, over those in Table 4. The higher densities derived by comparing only the highest frequency transitions of CS and H_2CO are probably unreliable. The densities derived from HCN make a more interesting case for higher densities since the uncertainties are less. Unfortunately, other transitions of HCN (e.g., $J = 2 \rightarrow 1$ and $J = 5 \rightarrow 4$) which would contribute to a full multitransition analysis are at frequencies where the atmospheric opacity is large.

This work was supported by National Science Foundation grant AST 83-12332 to the University of Texas at Austin.

REFERENCES

Erickson, N. 1981, *IEEE Trans.*, **MT29**, 557.
Kutner, M. L. 1978, *Ap. Letters*, **19**, 81.
Mundy, L. G. 1984, Ph.D. thesis, The University of Texas at Austin.
Mundy, L. G., Snell, R. L., Evans, N. J. II, Goldsmith, P. F., and Bally, J. 1986*a*, *Ap. J.*, **306**, 670.
Mundy, L. G., Evans, N. J. II, Snell, R. L., and Goldsmith, P. F. 1986*b*, submitted to *Ap. J.*
Ruze, J. 1966, *Proc. IEEE*, **54**, 633.
Snell, R. L., Erickson, N. R., Goldsmith, P. F., Ulich, B. L., Lada, C. J., Martin, R. N., and Schultz, A. 1986, *Ap. J.*, **304**, 780.
Snell, R. L., Mundy, L. G., Goldsmith, P. F., Evans, N. J. II, and Erickson, N. R. 1984, *Ap. J.*, **276**, 625.

JOHN H. DAVIS: Department of Electrical and Computer Engineering, The University of Texas at Austin, Austin, TX 78712

NEAL J. EVANS II: Department of Astronomy, The University of Texas at Austin, Austin, TX 78712

LEE G. MUNDY: Owens Valley Radio Observatory, California Institute of Technology, Pasadena, CA 91125

PAUL VANDEN BOUT: National Radio Astronomy Observatory, Edgemont Road, Charlottesville, VA 22903